INVESTIGATIONS OF OXYGEN ISOTOPE COMPOSITIONS COMBINED WITH Be-B AND Al-Mg SYSTEMATICS IN CV3 CAIs. E.T. Dunham[1], N.T. Kita[2], C. Defouilloy[2], S.B. Simon[3], M. Wadhwa[1] [1]Center for Meteorite Studies, Arizona State University, Tempe AZ, 85282 (email: etdunham@asu.edu), [2]Department of Geosciences, University of Wisconsin, Madison, Madison, WI, 53706, [3]Institute of Meteoritics, University of New Mexico, Albuquerque NM, 87131.

Introduction: The oxygen isotopic compositions of the oldest solids formed in the Solar System, the refractory calcium-, aluminum-rich inclusions (CAIs), span the entire range between solar and planetary compositions [1]. Although the phases in some relatively pristine CAIs record homogenous ^{16}O-rich compositions (i.e., close to the estimated solar composition [2]), most CAIs contain phases with compositions ranging from ^{16}O-rich to ^{16}O-poor [3]. Various models have been proposed to explain the oxygen isotopic compositions of phases in CAIs, including 1) evolution of the oxygen isotope composition of the nebular gas in the local environment where the CAI was forming; 2) physical transport of CAIs between distinct O isotopic reservoirs in the solar nebula during condensation or melting; 3) solid-state diffusion during nebular reheating; or 4) late isotopic exchange during parent-body aqueous alteration (e.g., [3]). To gain insights into if these processes were important in the formation of CAIs, it is important to correlate oxygen isotope compositions with other isotope systematics.

Here, we report the oxygen isotope systematics of four CAIs, for which the ^{10}Be-^{10}B and ^{26}Al-^{26}Mg systematics have been previously reported. The ^{26}Al-^{26}Mg short-lived chronometer (half-life ~0.7 Ma) has been applied extensively to early-formed Solar System materials [4]; the canonical value of the initial ^{26}Al/^{27}Al determined for normal CAIs is 5.2×10^{-5} (e.g., [5]). Beryllium-10 decays to ^{10}B with a half-life of 1.4 Ma and is almost exclusively formed by irradiation, most likely via collision of high energy solar particles with ^{16}O in CAI precursor materials. Previous studies show that CAIs have a range of initial ^{10}Be/^{9}Be ratios of ~10^{-4}-10^{-2} [e.g., 4]. As such, investigations of O isotopes combined with ^{10}Be-^{10}B and ^{26}Al-^{26}Mg systematics have the potential to provide information about the astrophysical environment in which the inclusions formed, as well as their chronology and alteration histories.

Samples: Four igneous CAIs from different CV3 meteorites were studied:

CAI B4 (NWA 6991, CV3$_{ox}$) is a compact type A (CTA) inclusion (~10 mm in the longest dimension) mainly composed of coarse melilite grains (~Åk$_{4-61}$), along with fassaite, spinel and minor anorthite; secondary alteration is only a minor component of B4 [6-8]. This inclusion has an ancient absolute Pb-Pb age of 4567.94 ± 0.31 Ma [7], well-behaved ^{26}Al-^{26}Mg systematics corresponding to a near-canonical $(^{26}Al/^{27}Al)_0$ ratio [5], and a $(^{10}Be/^{9}Be)_0$ ratio of $(6.8\pm2.8)\times10^{-4}$ [9].

CAI Agave (NWA 5028, CV3$_{red}$) is a type B2 inclusion (~5 mm across) dominated by fassaite, which encloses patches of melilite (Åk$_{1-85}$) and anhedral spinel; only minimal alteration products are present. This inclusion has a $(^{10}Be/^{9}Be)_0$ ratio $(1.3\pm0.5)\times10^{-3}$ and a $(^{26}Al/^{27}Al)_0$ ratio of $(4.99\pm0.02)\times10^{-5}$ [10].

CAI Saguaro (NWA 5508, CV3) is a spherical type B2 inclusion (~18 mm diameter) composed predominately of melilite (~Åk$_{30-65}$), with fassaite, spinel, and anorthite. Spinel is often distributed as rounded palisade bodies surrounding melilite, fassaite, and spinel [11]. Saguaro includes minimal alteration products and recorded a $(^{10}Be/^{9}Be)_0$ of $(8.2\pm2.0)\times10^{-4}$ [12].

CAI TS23 (Allende, CV3$_{ox}$) is a type B1 inclusion (~10 mm in diameter) composed of melilite (~Åk$_{5-25}$), fassaite, pyroxene, and spinel; it includes some minor secondary anorthite. The $(^{26}Al/^{27}Al)_0$ in TS23 is estimated to be 4×10^{-5} [13], and it has a high $(^{10}Be/^{9}Be)_0$ of $(6.1\pm0.8)\times10^{-3}$ [10].

Methods: In-situ oxygen isotope analyses of spinel, melilite, pyroxene, and anorthite in the four CAIs were performed during a single session with the Cameca IMS 1280 secondary ion mass spectrometer (SIMS) at the WiscSIMS laboratory at UW-Madison. Analytical conditions were similar to those reported using three Faraday cups (FC) [14]. The primary Cs^+ beam was 0.8 nA with a ~10 μm diameter and the secondary $^{16}O^-$ beam intensity was ~1×10^9 cps. We used a 10^{12} ohm resistor for the FC amplifier board for ^{17}O to improve analytical precision. San Carlos olivine was used as a standard and bracketed the unknown CAI analyses. Instrumental biases were corrected from the analyses of pyroxene (TiO_2: 2%, 10%), melilite (åkermanitic and gehlenitic), anorthite, and spinel standards at the beginning of the session. The 2σ errors for $\Delta^{17}O$ ($= \delta^{17}O - 0.52 \times \delta^{18}O$) were typically ±0.5‰. After the SIMS session, SEM images were taken of the spot analyses; none overlapped visibly with pits or cracks.

Results: Spinel and fassaite in each of these CAIs have relatively uniform ^{16}O-rich signatures ($\Delta^{17}O$ ~-23‰), while anorthite defines a range from somewhat ^{16}O-rich to ^{16}O-poor compositions, and melilite has a relatively uniform ^{16}O-poor composition (Fig. 1).

The ^{10}Be-^{10}B and ^{26}Al-^{26}Mg systematics in each of these CAIs were previously reported [10,12,16]. Figure 2 shows a plot of the $\Delta^{17}O$ estimated for the reservoir

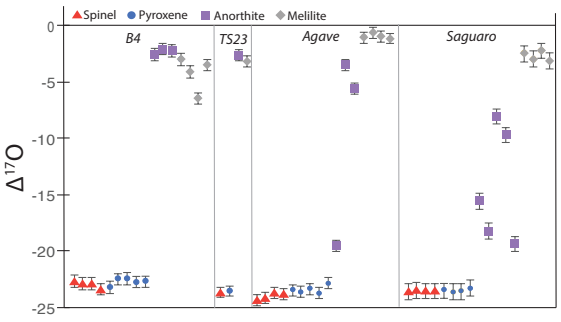

Figure 1: $\Delta^{17}O$ data for each analysis on CAIs B4, TS23, Agave, and Saguaro. Spinel = red triangles, pyroxene = blue circles, anorthite = purple squares, and melilite = gray diamonds. Error bars are 2σ from counting statistics.

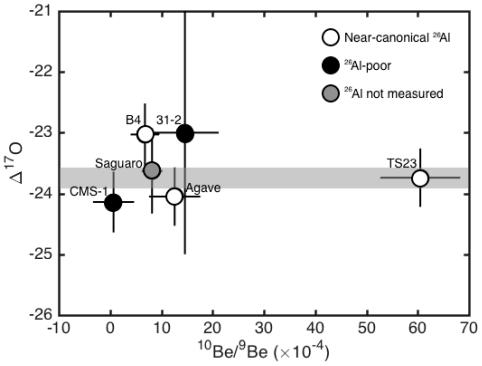

Figure 2: $\Delta^{17}O$ versus $^{10}Be/^{9}Be$ ratios; see text for explanation. The gray bar represents the $\Delta^{17}O$ weighted average of all 6 CAIs.

from which each CAI was originally formed (taken to be the average of the $\Delta^{17}O$ values measured here for the primary spinel) versus the inferred initial $^{10}Be/^{9}Be$ ratio. The B4, Agave, and TS23 inclusions have close to canonical ^{26}Al abundances; ^{26}Al has not yet been measured in the CAI Saguaro. Two additional ^{26}Al-poor CAIs (CMS-1 and 31-2) are also shown in Fig. 2 since O isotopes, as well as Be-B and Al-Mg isotope systematics have been reported for these inclusions as well ([16] and references therein).

Discussion: As can be seen in Fig. 2, there is no correlation between the $\Delta^{17}O$ values and the inferred initial $^{10}Be/^{9}Be$ or $^{26}Al/^{27}Al$ ratios. While there is a significant range in the $(^{10}Be/^{9}Be)_0$ ratios ($\leq 4\times10^{-4}$ to 6×10^{-3}) and $(^{26}Al/^{27}Al)_0$ (near-canonical ^{26}Al to ^{26}Al-poor), the $\Delta^{17}O$ values estimated for the nebular reservoirs for the CAIs considered here are similar within error (weighted average of -23.8±0.1‰). These observations support the hypothesis that ^{10}Be was predominantly produced via irradiation in a solar nebular reservoir characterized by a relatively uniform $\Delta^{17}O$ value. They further indicate that the variation in the inferred $(^{10}Be/^{9}Be)_0$ ratios is not due to secondary events. Since Mg has a faster diffusion rate than B in silicates [18], the nearly-canonical $(^{26}Al/^{27}Al)_0$ in the four CAIs studied here suggest that the ^{10}Be-^{10}B systematics were not significantly disturbed. There is additional mineralogic and geochemical evidence to suggest that the ^{10}Be-^{10}B systematics in the two other ^{26}Al-poor inclusions are also undisturbed [16].

Finally, while the ^{16}O-rich signature in the early-formed spinel is indeed indicative of the nebular reservoir in which the CAIs studied here began forming, the range of $\Delta^{17}O$ in the anorthites as well as the ^{16}O-poor composition of the melilites (Fig. 1) can be interpreted in one of two ways:

(1) The four igneous CAIs crystallized from an ^{16}O-rich nebular reservoir, but later (subsolidus) exchange with an ^{16}O-poor reservoir (in the nebula, or on a parent body) caused the differences in $\Delta^{17}O$ between spinel, melilite, and anorthite; these phases are variably susceptible to such exchange, with spinel being the most robust [19]. If this exchange was with nebular gas, it likely occurred at the edge of the disk (suggested location of the ^{16}O-poor reservoir [3]). However, irradiation production of ^{10}Be occurred most efficiently in the ^{16}O-rich region near the midplane, close to the violent proto-Sun. Since the ^{16}O-poor melilite shows clear evidence for the presence of live ^{10}Be, this phase likely did not crystallize in CAIs at the edge of the disk. As such, subsolidus exchange with a ^{16}O-poor fluid on parent body is most probably the cause of the distinct $\Delta^{17}O$ values in the melilite compared to the spinel.

(2) Alternatively, the oxygen isotopic composition of the nebular reservoir changed dramatically during the crystallization of CAI phases. Some recent studies [3,17] suggest that the O isotope composition of the nebular environment changed dramatically during crystallization of fassaite in igneous (type B1) CAIs. A similar process may have occurred during anorthite crystallization, but further work is required to better evaluate this possibility.

Acknowledgments: This work is supported by a NASA Earth and Space Science Fellowship (NNX16AP48H) to ED and a NASA Emerging Worlds grant (NNX15AH41G) to MW.

References: [1] MacPherson G.J. (2014) *Treatise on Geochemistry (2nd Ed.),* p.139. [2] McKeegan K.D. et al. (2011) *Science 322*, 1528. [3] Aleon J. (2016) *EPSL 440*, 62. [4] Davis A.M. & McKeegan K.D. (2014), *Treatise on Geochemistry (2nd Ed.),* p.361. [5] Jacobsen B. et al. (2008) *EPSL 272*, 353. [6] Bouvier, A. et al. (2011) *Workshop on Formation of the First Solar System Solids,* Abstract #9054. [7] Wadhwa, M. et al. (2014) *LPS 45,* Abstract #2698. [8] Bullock E. et al. (2014) *LPS 45,* Abstract #1919. [9] Dunham E.T. et al. (2017) *LPS 48*, Abstract #1507. [10] Dunham E.T. et al. (2016) *MetSoc,* Abstract #6222. [11] Simon S.B. and Grossman L. (1997) *MAPS 32*, 61. [12] Dunham E.T. et al. (2017) *MetSoc,* Abstract #6381. [13] Hutcheon I. (1982) *ACS 176*, 95. [14] Kita N.T. et al. (2010) *GCA 74*, 6610. [15] Yurimoto H. et al. (2008) *Reviews M&G 68*, 141. [16] Dunham E.T. et al. (2018) *this meeting,* Abstract #2402. [17] Kawasaki N. et al. (2018) *GCA 221*, 318. [18] Sugiura N. et al. (2001) *MAPS 36,* 1397. [19] Ryerson F.J. and McKeegan K.D. (1994) *GCA 58*, 3713.